Supporting Information for *Vivid, Full-Color Aluminum Plasmonic Pixels*

Jana Olson, Alejandro Manjavacas, Lifei Liu, Wei-Shun Chang, Benjamin Foerster, Nicholas King, Mark W. Knight, Peter Nordlander, Naomi J. Halas, and Stephan Link

Correspondence to: halas@rice.edu, slink@rice.edu

This file includes:

Table S1: A complete list of all physical parameters for the pixels discussed in the full text.

		a	b	c	d	e	f
1	length (nm)	155	135	105	95	90	85
	Dx (nm)	180	180	180	180	180	180
	Dy (nm)	290	270	240	230	225	220
	Γ	140	140	140	140	140	140
	#rods	459	486	540	567	594	594
2	length (nm)	155	135	105	95	90	85
	Dx (nm)	210	210	210	210	210	210
	Dy (nm)	320	300	270	260	255	250
	Γ	170	170	170	170	170	170
	#rods	345	368	414	437	437	460
3	length (nm)	155	135	105	95	90	85
	Dx (nm)	240	240	240	240	240	240
	Dy (nm)	350	330	300	290	285	280
	Γ	200	200	200	200	200	200
	#rods	280	300	320	340	340	340
4	length (nm)	155	135	105	95	90	85
	Dx (nm)	270	270	270	270	270	270
	Dy (nm)	380	360	330	320	315	310
	Γ	230	230	230	230	230	230
	#rods	234	234	270	270	270	288
5	length (nm)	155	135	105	95	90	85
	Dx (nm)	300	300	300	300	300	300
	Dy (nm)	410	390	360	350	345	340
	Γ	260	260	260	260	260	260
	#rods	192	192	208	224	224	224
6	length (nm)	155	135	105	95	90	85
	Dx (nm)	330	330	330	330	330	330
	Dy (nm)	440	420	390	380	375	370
	Γ	290	290	290	290	290	290
	#rods	165	165	180	195	195	195
7	length (nm)	155	135	105	95	90	85
	Dx (nm)	360	360	360	360	360	360
	Dy (nm)	470	450	420	410	405	400
	Γ	320	320	320	320	320	320
	#rods	130	143	143	156	156	156

This table is organized so as to match Fig. S4 in the supporting information; a1 is the top left pixel in the image, and f7 is the bottom right pixel in the image.

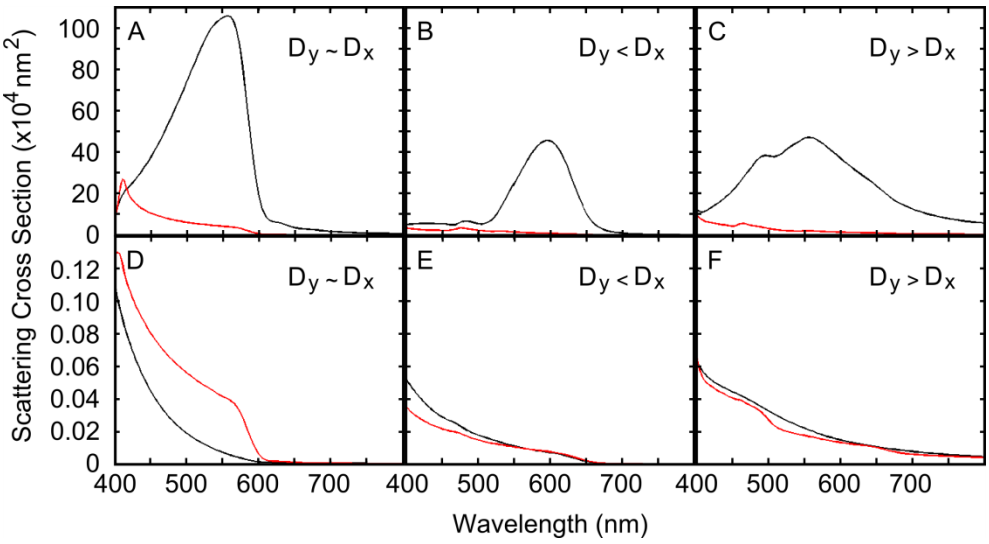

Fig. S1. Calculated Scattering spectra of pixels composed of nanorods with physical dimensions l = 95 nm, w = 40 nm, and h = 35 nm (*A* - *C*) and nanospheres with a diameter of 30 nm (*D*-*F*) collecting the response to either the p-polarized excitation (black) or the s-polarized excitation (red). Both (*A*) and (*D*) have D_y = 290 nm and D_x = 240 nm, representing values for D_y/D_x found in the main text. The nanorod based pixel demonstrates stronger response to different polarized excitation than spheres in this D_y/D_x regime. The sdame behavior is also seen when D_y = 190 nm and D_x = 990 nm (*B, E*), and when D_y = 990 nm and D_x = 190 nm (*C, F*). We conclude that the spheres demonstrate very little polarization dependence, regardless of the values chosen for D_y and D_x. These calculations were performed with an average refractive index of n = 1.55, excitation incident at 53° with p- (black lines) or s- (red lines) polarization. In all cases, the field intensity is chosen to give the same in-plane amplitude. We assign the strong polarization dependence to the anisotropic polarizability of the nanorods.

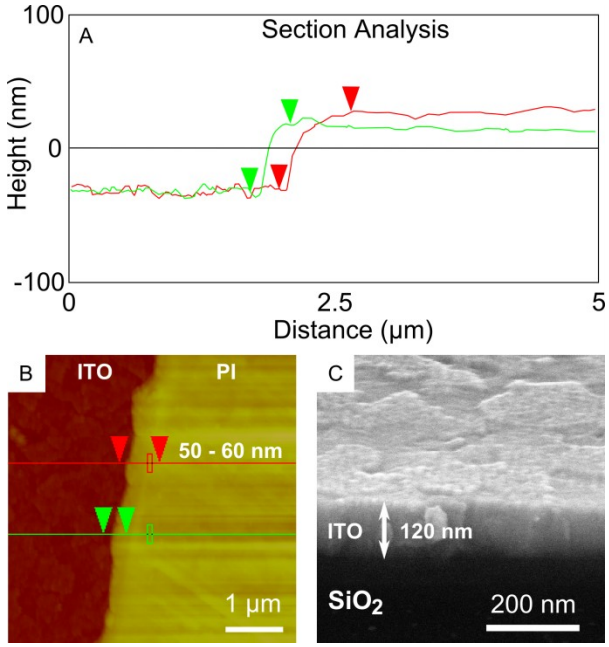

Fig. S2. Thickness data for both PI and ITO layers of the sample substrate. (*A*) A section analysis of an atomic force microscope (AFM, Digital Instrument Nanoscope IIIA) image (*B*) performed using tools in the AFM software. The AFM image shows a scratch test of a sample slide with bare ITO on the left side and PI on the right side. The striations are an effect of the 1st order flattening process performed on this image using standard AFM software, and therefore two thickness measurements were performed on the same image, showing similar measurements of a polyimide thickness of 50 to 60 nm. AFM surface roughness measurements, provide average surface roughness values for bare ITO (2.636 nm), PI on ITO (0.636 nm), and PI on a lithographically prepared pixel (0.984 nm). Coating the plasmonic pixels with polyimide hence reduces the surface roughness by 2 to 4 times. This improved smoothness causes less background scattering and improves the signal to noise ratio. (*C*) SEM image showing an edge section of an ITO coated slide with no polyimide. This sample was mounted on a 70° tilted sample stage and imaged at 400,000 x magnification at 10 mm working distance. The ITO

thickness is approximately 120 nm, which is too thin to act as an efficient dielectric waveguide to excite the aluminum pixels.

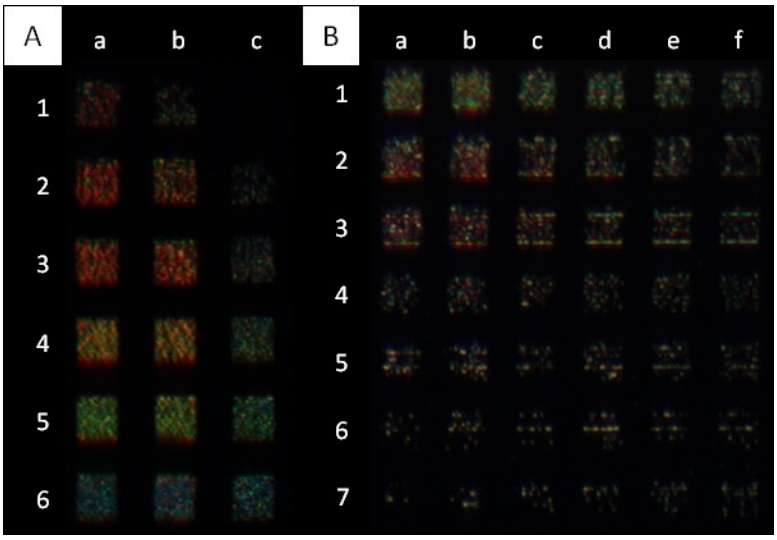

Fig. S3. Polarized DSLR camera images of pixel arrays prepared with randomized nanorod positions rather than well-ordered arrays, excited under both p- and s-polarized light propagating along the *yz* plane. *(A) y*-polarized image of 5 μm x 5 μm pixels where the nanorods within each pixel are positioned by first creating a square array, and then perturbing the *x* and *y* positions of each nanorod by a random amount. No nanorods are allowed to come within 30 nm of each other to prevent near-field coupling. Nanorod lengths are 155 nm (column a), 130 nm (column b), and 105 nm (column c), and the number of nanorods in each pixel is 144 nanorods (row 1), 196 nanorods (row 2), 225 nanorods (row 3), 289 nanorods (row 4), 324 nanorods (row 5), and 400 nanorods (row 6). The DLSR camera exposure time is 4 seconds. *(B)* Same pixel design as defined in Table S1, but with 10% of the nanorods in each pixel randomly shifted in the *y* direction by no more than the length of the nanorod. The DLSR camera exposure time is 5 seconds. Both of these images, taken with comparable exposure times, demonstrate that pixels with randomized nanorod positions are not as bright as well-ordered arrays. Although the pixels in (*A*) and (*B*) seem to have some color tunability with variations in the nanorod density, both examples show mosaic-like patterns instead of homogeneously distributed colors like the well-ordered arrays.

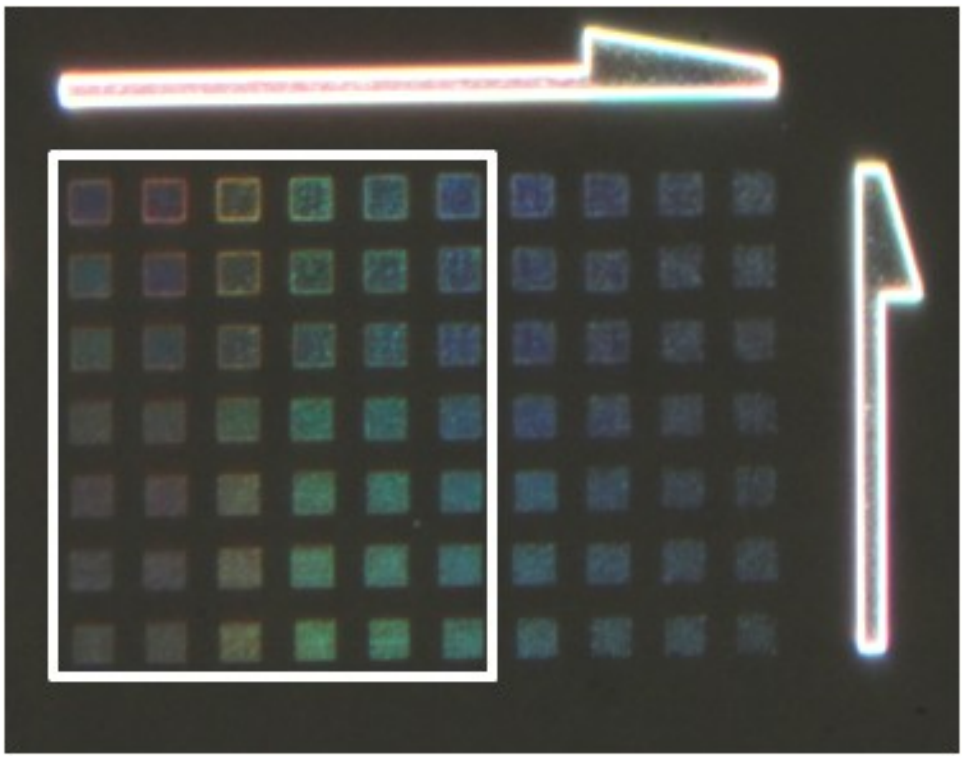

Fig. S4: Reflected light dark field image of the same pixel array described in the text. The contrast and brightness of this image have been significantly adjusted to make the pixels more visible. The region inside the box corresponds to the same array as included in the main text, and the nanorod length l, D_x, and D_y are provided in Table S1. With this reflected light excitation scheme, using a 50x objective (NA = 0.8) with a drop of oil on the glass side of the sample to reduce background, the increasing nanorod length red-shifts the color of the pixel (from right to left in the image), but decreasing the period (from top to bottom) serves only to add some slight intensity and does not appear to contribute to any color tuning. This image shows that different excitation conditions can significantly change the color of the pixels, as well as the color tunability from D_x and D_y, as in this case here diffractive coupling is suppressed.

Theoretical model

The theoretical calculations are performed using a coupled dipole model [1,2]. Within this approach, the nanorods are described as point dipoles with anisotropic polarizability $\alpha = \alpha_{xx}\hat{\mathbf{x}}\hat{\mathbf{x}} + \alpha_{yy}\hat{\mathbf{y}}\hat{\mathbf{y}} + \alpha_{zz}\hat{\mathbf{z}}\hat{\mathbf{z}}$. This polarizability is obtained through a Finite Element Method (FEM) simulation performed using the commercial software COMSOL Multiphysics. When the ensemble is illuminated with an external field $\mathbf{E}(\mathbf{r})$, the dipole induced in each nanorod can be written as

$$\mathbf{p}_i = \alpha\left(\mathbf{E}(\mathbf{r}_i) + \sum_j \mathbf{G}_{ij}\mathbf{p}_j\right).$$

Here, $\mathbf{G}_{ij} = [k^2 + n^{-2}\nabla\nabla]\exp(ikn|\mathbf{r}_i - \mathbf{r}_j|)/|\mathbf{r}_i - \mathbf{r}_j|$ is the dipole-dipole interaction matrix, $\mathbf{r}_i$ are the vectors with the nanorod positions, k is the light wavevector in vacuum, and n is the refractive index surrounding the nanorod ensemble. The self-consistent induced dipole can be obtained by solving this system of equations as

$$\mathbf{p}_i = \sum_j \mathbf{M}_{ij}^{-1}\alpha\mathbf{E}(\mathbf{r}_j),$$

where $\mathbf{M}_{ij} = [\delta_{ij} - \alpha\mathbf{G}_{ij}]$. Finally, the power scattered by the nanorod ensemble is given by

$$P = \frac{cnk^4}{2\pi}\mathrm{Re}\sum_{i,j}\int d\Omega \mathrm{e}^{ikn(\mathbf{r}_j - \mathbf{r}_i)\cdot\hat{\mathbf{s}}}[\mathbf{p}_i \cdot \mathbf{p}_j^* - (\mathbf{p}_i \cdot \hat{\mathbf{s}})(\mathbf{p}_j^* \cdot \hat{\mathbf{s}})].$$

Here, $\hat{\mathbf{s}}$ is the unit vector in the radial direction, and the angular integral is performed over the angles compatible with the numerical aperture of the detection set up.

In order to test the accuracy of the coupled dipole model we have compared it with the rigorous solution of Maxwell's equations obtained through FEM simulations performed with the COMSOL Multiphysics software. The system chosen for this test consists of an ensemble of 4

nanorods with $l = 95$ nm, $w = 40$ nm, and $h = 35$ nm, separated by $D_x = 240$ nm and $D_y = 290$ nm, and embedded in a medium with a refractive index $n = 1.55$. Notice that this system, contrarily to the ensembles considered in the main paper, is within the limits of what can be simulated using FEM. Fig. S5 shows the scattering produced by the ensemble when illuminated at normal incidence with an electric field polarized along the long axis of the nanorods. The black line represents the results of the coupled dipole method while the red curve corresponds to FEM simulations. As can be seen from Fig. S5, there is a good agreement between both methods, especially in the position of the resonance peak.

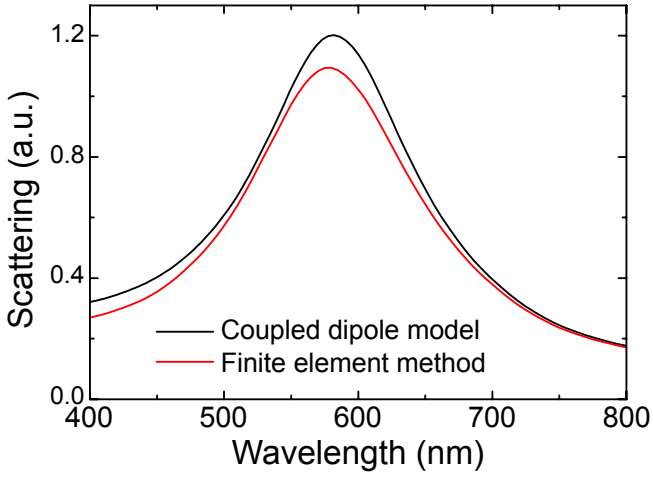

Fig. S5: Comparison between the scattering spectrum calculated with the coupled dipole model (black line) and the corresponding one obtained from the rigorous solution of Maxwell's equations with a Finite Element Method simulation (red line). The system studied consists of an ensemble of 4 nanorods with $l = 95$ nm, $w = 40$ nm, and $h = 35$ nm, separated by $D_x = 240$ nm and $D_y = 290$ nm, and embedded in a medium with a refractive index $n = 1.55$. The incident field is normal to the sample plane and polarized along the long axis of the nanorods.

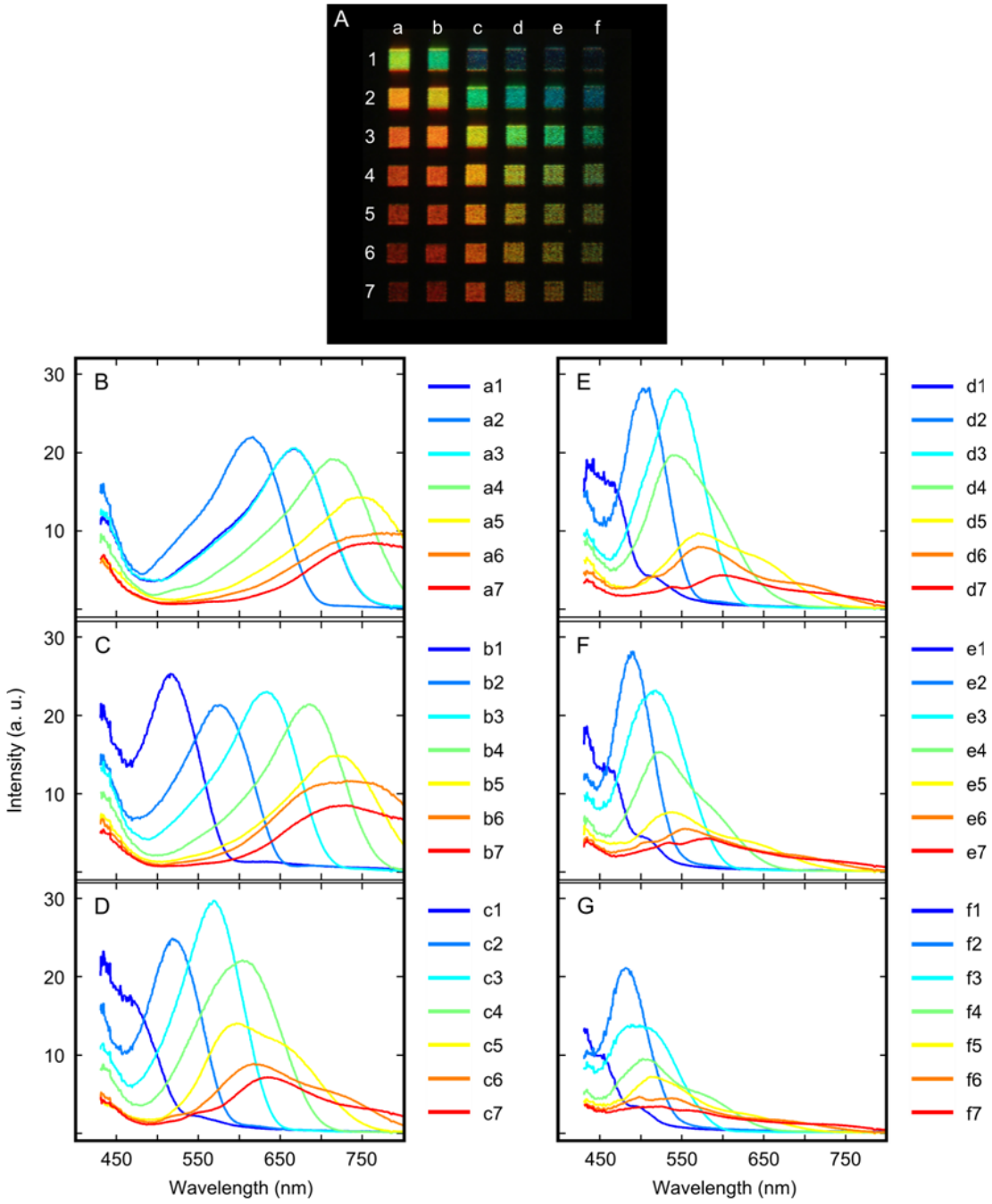

Fig. S6: Dark field spectra of all pixels shown in manuscript text. Seven pixels, with variable D_x and D_y, were prepared for each nanorod length, according to the row and column labels shown in *(A)* and also matching the indices for the Table S1*: (B)* l = 155 nm, *(C)* l = 135 nm, *(D)* l = 105 nm, *(E)* l = 95 nm, *(F)* l = 90 nm, *(G)* l = 85 nm. All spectra were taken with an integration time of 40 seconds, and corrected by subtracting background and dividing by a transmission spectrum

of the excitation lamp. The nanorod length, D_x, D_y, and the number of nanorods in each pixel are given in Table S1. The full spectrum from 430 nm to 800 nm is presented here. Importantly, the noise increases on the left side of the spectra, toward 400 nm, primarily because of the low lamp intensity in this region, though the efficiency of the detector is also reduced in this region compared to longer wavelengths.

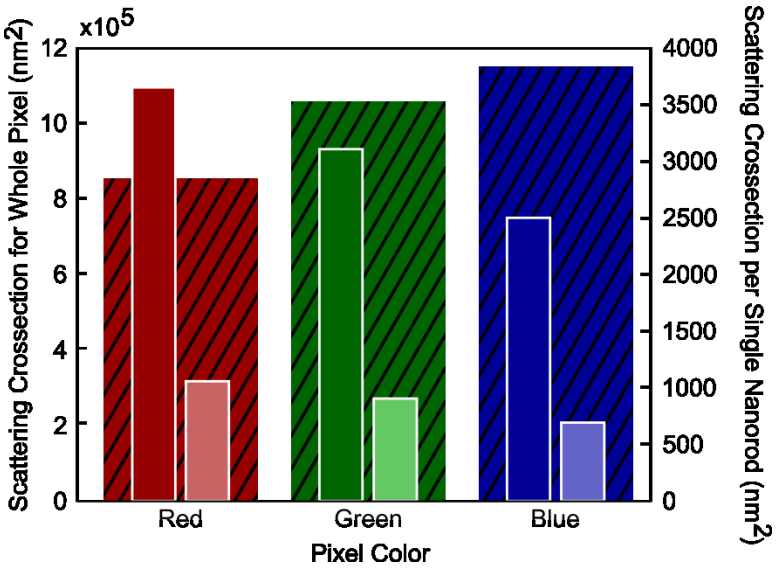

Fig. S7. Calculated scattering cross sections of red, green, and blue pixels (black-striped wide bars, left axis); scattering cross sections for the same three pixels, divided by the number of nanorods in each pixel (dark colored narrow bars, right axis); and scattering cross sections for single, non-interacting nanorods of the same physical dimensions as are used in their respective pixels (light colored narrow bars, right axis). The values plotted in this graph are for 680 nm (red, 234 rods), 556 nm (green, 340 rods), and 489 nm (blue, 460 rods), which are the peak scattering cross sections from the calculated spectra in Fig. 3 in the main text. The relative heights of the light and dark narrow bars show that the strong scattering cross section of these pixels is more than three times the value of a single non-interacting nanorod, when accounting for the number of nanorods in a single pixel. When the scattering cross section of the whole pixel is considered (striped bars), then it is clear that a larger nanorod density increases the intensity of the pixel, illustrating that both diffractive coupling and density of scatterers play a role in determining the resulting intensity of a plasmonic pixel.

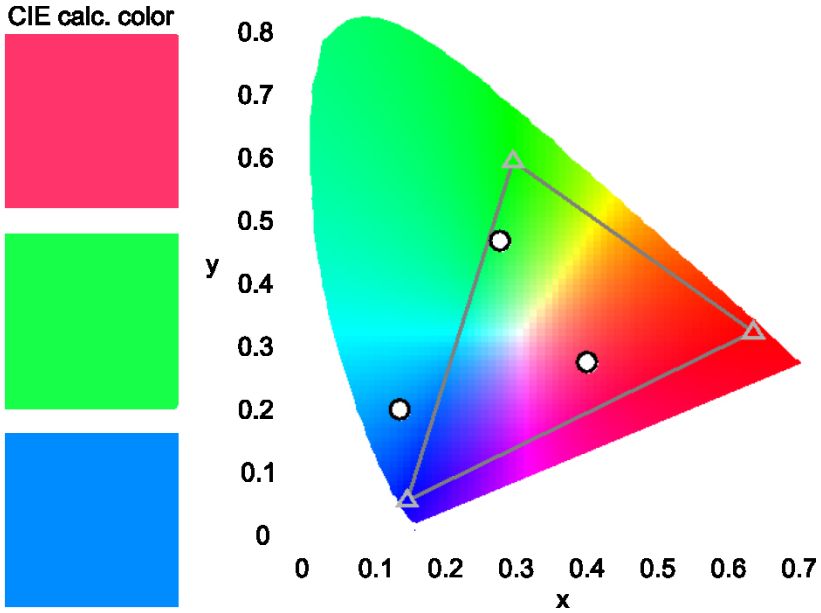

Fig. S8. Left: Color obtained from the experimental red, green, and blue spectra shown in Fig 3A of the text using CIE 1931 standard observer. Right: Chromaticity graph showing the RGB color gamut (gray lines connecting the red, green, and blue tristimulus values, shown as triangles) and the CIE coordinates (circles) for the three pixels. The x and y coordinates correspond to the color's hue, while the z axis (normal to the xy plane) corresponds to the brightness of the color. The same method of CIE color calculation was used as in Fig. 3, and the small deviation of the color between the digital camera image (Fig. 3) and the colors calculated from the experimental spectra is caused by the color-correction software that comes pre-installed on the digital camera.

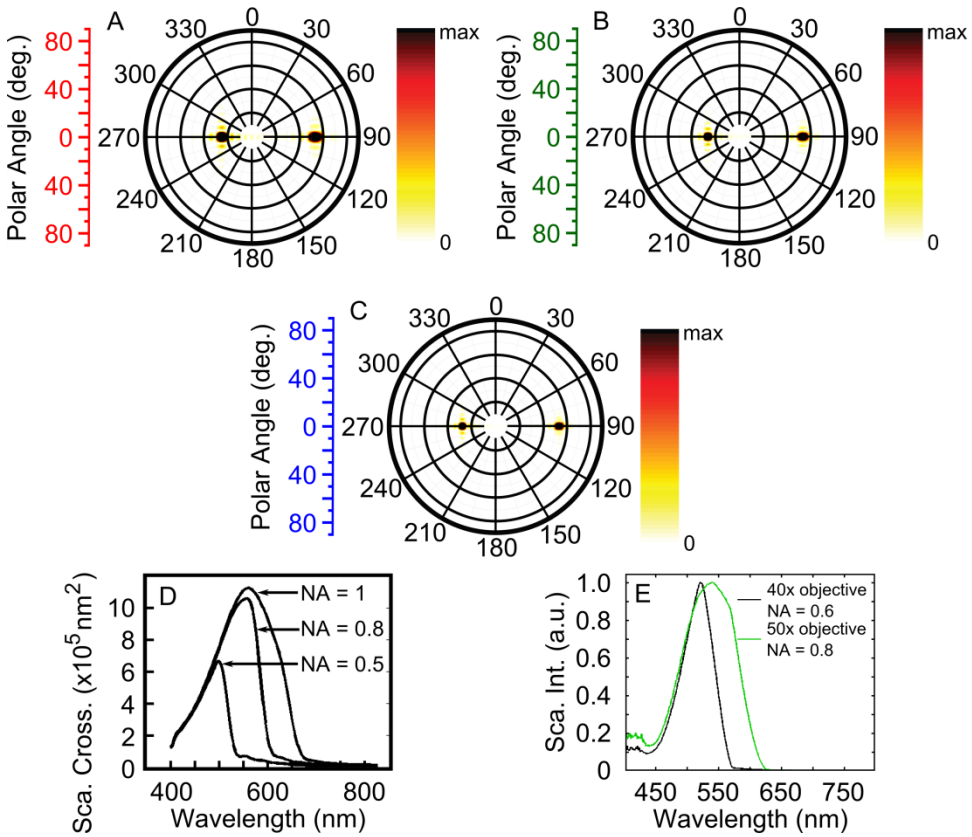

Fig. S9. Angular dependence of pixel scattering. (*A*) Polar plot of the angular distribution of the peak wavelength scattering cross section of the red pixel, excited by p-polarized white light incident from the 270° azimuthal angle at 53° polar angle. Essentially, the pixel is "located" at the center of the graph, with nanorod long axes parallel to the 270°/90° azimuthal angle, and the sample surface is parallel to the plane of the graph. The sample is excited from the left at a polar angle of 53°, and a spatial intensity map for the peak wavelength shows a forward scattered and a backscattered peak. The red pixel scatters at a peak wavelength of 680 nm. The backscattered peak near 25° along the 270° azimuthal angle is the peak that is collected by the objective (which has a collection angle of 30°) in our experimental set up. The forward scattered peak that lies at azimuthal angle 90° and 45° polar angle is not collected by the objective. Similar peaks are also observed for (*B*) the green pixel, which has a scattering peak at 556 nm, and (*C*) the blue pixel, which scatters with a peak at 489 nm. (*D*) The green pixel was simulated with three different

collection angles, 20°, 30°, and 40° (assuming a refractive index of 1.55 for polyimide), which represent three different NA objectives: NA = 0.5, 0.8, and 1, respectively. These simulations demonstrate that larger collection angles allow longer wavelengths to be collected and observed. Note that the critical angle for the polyimide-air system is just smaller than 40°, and so wavelengths that are scattered with larger angles will be totally internally reflected at the interface and cannot be collected by an air-space objective experimentally. (*E*) Experimentally verification of the behavior illustrated in (*D*) using NAs of 0.6 and 0.8.

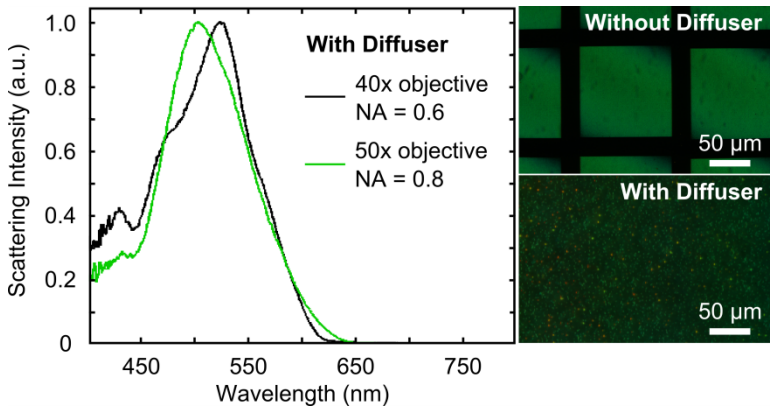

Fig. S10. Experimental scattering spectra of a green pixel with a commercially available diffuser layer taken with NAs of 0.6 and 0.8. An area of approximately 0.4 mm was patterned with 100 μm square pixels with l = 95 nm, D_x = 240 nm, and D_y = 290 nm, and the sample was coated with PI. A sample of commercially available plastic diffuser film was attached to the sample using double sided tape, with the roughened side of the film facing the pixels. The tape held the diffuser in place while also preventing the diffuser surface from contacting the PI. Spectra were taken using a 40x objective with NA = 0.6 (black line), and also using the 50x objective with NA = 0.8 that was described in the main text (green line). Unlike the spectra shown in Fig. S9E, with the diffuser in place the spectra of the green pixel collected using the two different objectives are very similar, and produce a color that matches the pixels imaged without the diffuser as illustrated by the images on the right. The highly directional scattering caused by the diffractive coupling (Fig S9) can therefore be mitigated by including a diffuser layer that redirects light in all directions so that the pixel color remains uniform independent of collection cone, i.e. viewing angle. Unlike shown here, diffusers can also be patterned to match the size of the pixels, so as to preserve the spatial footprint of individual pixels and to avoid mixing of colors from nearby different pixels.

References

1. Zhao L, Lance Kelly K, & Schatz GC (2003) The extinction spectra of silver nanoparticle arrays: influence of array structure on plasmon resonance wavelength and width. *J. Phys. Chem. B* 107:7343-7350.

2. García de Abajo, FJ (2007) Colloquium: Light scattering by particle and hole arrays. *Rev. Mod. Phys.* 79:1267-1290.